Geogr. Fis. Dinam. Quat.
36 (2013), 63-80, 11 figg., 1 tab.

DOI 10.4461/GFDQ.2013.36.5

JOACHIM GÖTZ (*), JAN-CHRISTOPH OTTO (*) & LOTHAR SCHROTT (*)

POSTGLACIAL SEDIMENT STORAGE AND ROCKWALL RETREAT IN A SEMI-CLOSED INNER-ALPINE SEDIMENTARY BASIN (GRADENMOOS, HOHE TAUERN, AUSTRIA)

ABSTRACT: GÖTZ J., OTTO J.C. & SCHROTT L., *Postglacial sediment storage and rockwall retreat in a semi-closed inner-Alpine sedimentary basin (Gradenmoos, Hohe Tauern, Austria)*. (IT ISSN 0391-9838, 2013).

This study quantifies postglacial sediment storage in the Gradenmoos basin – a glacially over-deepened, semi-closed sedimentary basin (4.5 km^2) in the central Gradenbach catchment (32 km^2, Schober Mountains, Carinthia, Austrian Alps) – and reconstructs rates of postglacial rockwall retreat and mechanical denudation. The topographic setting of the basin facilitates the reconstruction of small-scale postglacial landscape evolution since clastic sediment removal can be neglected due to lake existence over 7,500 years after Younger Dryas deglaciation (Egesen). Furthermore, source areas are clearly delineated and intermediate sediment storage is low due to short source-sink distances and steep slope gradients. Sediment storage volumes are quantified using high-resolution surface (terrestrial laser-scanning, geomorphological mapping) and subsurface information (geophysical prospection, core drilling). These data are an input for GIS-based bedrock interpolation and 3-D modelling of sediment storage. The timing of sedimentation and rockwall retreat after deglaciation and the amount of basal till deposits underneath present-day landforms are estimated using core drilling, stratigraphic analyses, palynological observation, and AMS ^{14}C dating. Total (postglacial) sediment storage within and surrounding the basin amounts to 19.7 (18.3) x 10^6 m^3 whereas hillslope storage overbalance basin fill deposits by a factor of five. Rockwall retreat rates of less than 520 mm/ka, however, indicate comparatively low values despite of steep slope gradients and coarse and blocky weathering conditions in the area. The study presents a new and almost complete small-scale sediment budget approach, provides postglacial rates of rockwall retreat for the eastern Alps, and copes with several uncertainties disregarded in previous studies. For the first time, several uncertainties are quantitatively addressed, such as pre-Holocene basal till underneath present-day landforms, re-deposited sediment volumes, and the absolute timing of the period available for postglacial sedimentation and denudation.

KEY WORDS: Postglacial, Geomorphological mapping, Near-surface geophysics, Sediment storage, Rockwall retreat, Hohe Tauern (Austria).

INTRODUCTION

Alpine sediment production, storage and routing can be interpreted as a result of geomorphological processes operating with variable frequencies and magnitudes in an altering and complex topographic setting. Altitudinal limits, for instance equilibrium line altitudes, permafrost or vegetation limits, or elevation ranges of intensified frost shattering (Hales & Roering, 2005; Delunel & *alii*, 2010), shift in elevation as a consequence of climate change and thus modulate rate and type of erosion and sedimentation on longer time scales. Pleistocene glaciation, deglaciation, and effects of paraglacial landscape adjustment represent such climatically controlled factors severely modifying Alpine sedimentation (*e.g.*, Ryder, 1971 a, b; Ballantyne, 2002; Slaymaker, 2009). Additionally, high-magnitude climatic events also lead to infrequent sudden landscape changes on shorter time scales. The efficiency of these extrinsic, climatically controlled factors is additionally governed by topographic, lithologic, and tectonic parameters. Feedback mechanisms between these factors are still critically discussed. However, most basic relations of cause and effect between rock uplift, tectonic forcing, (glacio)

(*) *Salzburg Universität, Research Group Geomorphology and Environmental Systems, Hellbrunnerstraße 34, 5020 Salzburg, Austria*. E-mail: joachim.goetz@sbg.ac.at

Extensive fieldwork has been performed during different field courses and with the help of numerous volunteering students from the University of Salzburg. Their help is greatly appreciated. Special thanks to R. Krisai for palynological analysis, J. Buckel for assistance in the lab and in the field, J. Bellinger for geomorphological mapping efforts, C. Halla for stratigraphic analyses of the sediment cores, and G.K. Lieb for various discussions on the postglacial history of the study area. The authors thank further two anonymous referees for perceptive comments. The Kärntner Landesregierung/ Kagis and the national park Hohe Tauern kindly provided orthophoto and digital elevation data. This study is part of the Eurocores programme Topo-Europe of the European Science Foundation. Financial support from the Austrian Science Fund (FWF) [I00156-N19] is greatly appreciated. We dedicate this paper to Monique Fort on the occasion of her retirement.

isostatic rebound and denudational unloading remain not fully understood, particularly if variable levels of plate convergence between the eastern, central, and western Alps are considered (Champagnac & *alii*, 2009; Hergarten & *alii*, 2010).

Alpine denudation and rockwall retreat have been investigated on various spatial and temporal scales mainly using two approaches: (i) the measurement of in-situ produced cosmogenic nuclides in river and slope sediments (*e.g.*, Norton & *alii*, 2010; von Blanckenburg, 2006; Wittmann & *alii*, 2007), and (ii) the sediment budget approach that quantifies sediment fluxes based on sediment deposition in landforms and sinks that is related to the contributing area and the time-span of erosion. Whereas the integration time of the former approach is controlled by the denudation rate itself (typically high rates of Alpine denudation account for relatively short integration times not covering the entire Holocene), the time period of averaging is controlled by sedimentary archives if the latter approach is used. Sediment budget-derived rates of denudation and rockwall retreat have been quantified from sediment storage volumes with varying degrees of accuracy since different ways of volume quantification were applied ranging from simple visual estimation to geometrical modelling, drilling, coring, and detailed geophysical surveys (*e.g.*, André, 1997; Hinderer, 2001; Kuhlemann & *alii*, 2001; Hoffmann & Schrott, 2003; Curry & Morris, 2004; Cossart & Fort, 2008; Delmas & *alii*, 2009; Moore & *alii*, 2009; Otto & *alii*, 2009; Tunnicliffe & Church, 2011).

Sediment budget analyses explicitly address the quantification of sediment production, transfer, and storage within catchments (Jordan & Slaymaker, 1991; Reid & Dunne, 1996; Slaymaker, 2003). Depending on spatial and temporal scales, the approach can be applied bi-directional by quantifying sediment flux or volumes, whereas both measures can be derived from each other (Hinderer, 2012). The analyses of sedimentation and denudation within larger catchments are often based on the present-day sediment discharge and its relation to the hydrological catchment area (Schlunegger & Hinderer, 2003). This sediment delivery based approach implies that catchments are treated as black box models, that internal system configurations are neglected, and that the change in sediment delivery through time due to long-term variations and short-term scatter is disregarded. Besides, recent sediment discharge might be strongly affected by humans, particularly in densely populated and severely modified Alpine environments. The analysis of large-scale denudation-accumulation systems (peri-Alpine lakes, large valley fills) overcomes temporal variability by assessing averaged rates of postglacial denudation (Einsele & Hinderer, 1998; Müller, 1999; Hinderer, 2001; Hinderer & Einsele, 2001). However, besides the temporal scatter, these studies also average the spatial dimension or the degree to which specific source areas contribute to total sediment delivery and intermediate sediment storage is often disregarded. Few small-scale studies explicitly focused on internal system dynamics and intermediary sediment storage using geophysical techniques and GIS-based modelling approaches (Hoffmann & Schrott, 2002; Schrott & Adams, 2002; Schrott & *alii*, 2003; Otto & *alii*, 2009). These studies gained further control on spatial and temporal scales as volumes of intermediary sediment storage could be assessed. Remaining uncertainties in these types of investigations comprise (i) the quantity of evacuated sediment since deglaciation, (ii) initial amounts of glacigenic till deposits underneath present-day sediment storage landforms, and (iii) the absolute timing of deglaciation. Detailed small-scale sediment budgets within closed sedimentary systems, which minimise mentioned uncertainties, improve the interpretation of postglacial sedimentation and denudation in Alpine environments. These studies can benefit from the topographic effect of glacial erosion itself since glacial scouring often left over-deepened basins effectively trapping sediments since deglaciation. Additionally, lateglacial oscillations frequently evacuated large amounts of sediments leaving «empty basins» and thus reset «the clock of sedimentation». Such basins impact on catchment connectivity and account for sediment flux interruption, which is frequently expressed by characteristic knick points in longitudinal valley profiles. With different levels of recent infilling, these basins often archive complete postglacial stratigraphic records facilitating the reconstruction of Holocene landscape evolution. Accordingly, this study quantifies postglacial sediment storage and rockwall retreat within and surrounding the glacially over-deepened Gradenmoos basin (sub-catchment size: 4.5 km^2; basin floor elevation: 1920 m, Gradenbach catchment, Schober Range, Austrian Alps) using a combined field and a GIS-based modelling approach.

PHYSICAL SETTING

With a range in elevation from 1045 m (Putschall) to 3283 m (Peak Petzeck), the Gradenbach catchment (32 km^2) drains eastward into the River Möll (Carinthia, Austria). The valley bottom of the Möll River is climatically well shielded and characterised by continental conditions but continental pattern decreases towards higher elevations. Located nearby the Gradenbach valley outlet, the climate station of Döllach recorded an average annual precipitation of 826 mm/a and a mean annual air temperature of 6.1 °C (http://www.zamg.ac.at). Annual runoff of the Gradenbach river amounts to 25.3-36.3x10^6 m^3/a after a total flow length of 9 km with highest daily and monthly totals in June and July (gauging station Gradenwehr 1991-1996; Lang & Hagen, 1999). The catchment is deeply incised and surrounded by more than 20 peaks exceeding 3000 m in elevation and shows an asymmetrical cross-profile with steep north-facing rockwalls and more gentle south-facing slopes. The catchment is located within the heavily fractured Palaeozoic lithology («Altkristallin») southwest of Penninic Tauern Window formations and the Matrei zone composing the outermost part of the catchment (fig. 1, map 2). This metamorphic lithology is characterised by intensive, coarse and blocky weathering conditions.

The Schober Mountain Range, and particularly the Gradenbach catchment, shows a distinct glacial signature

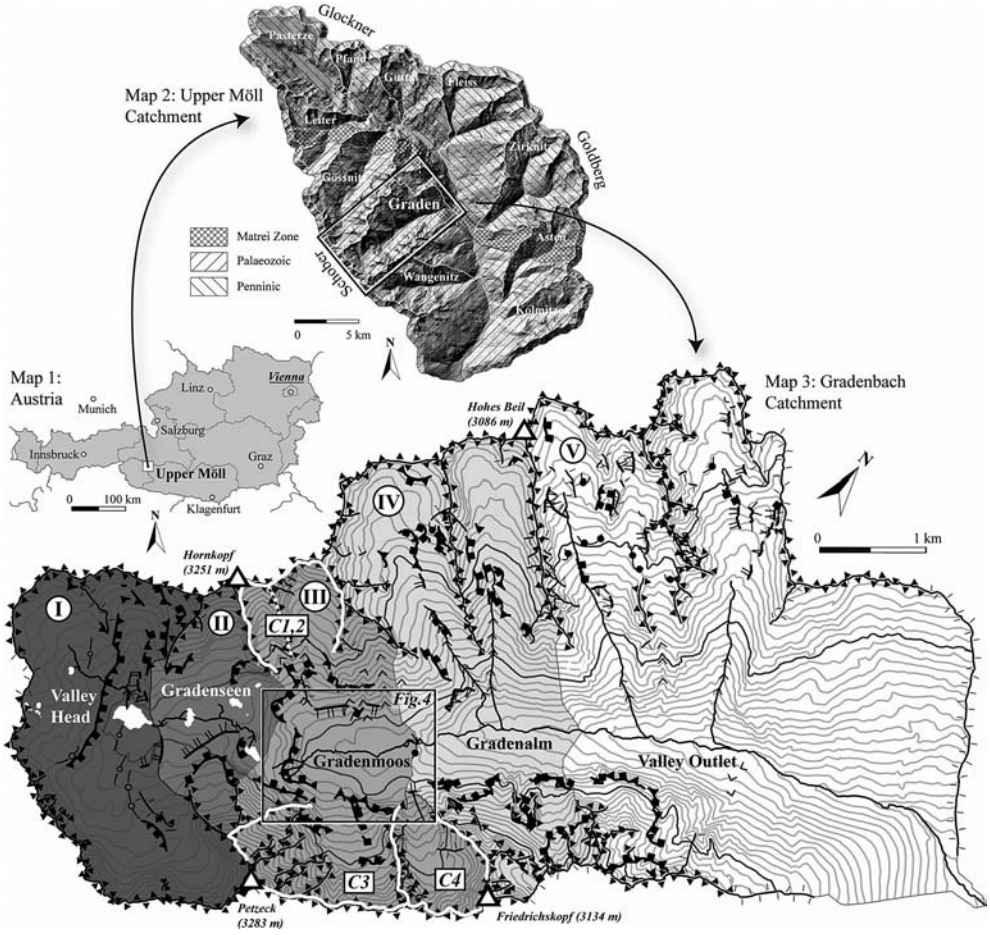

FIG. 1 - The Gradenbach catchment (map 3) as a part of the upper Möll catchment (map 2) within Austria (map 1). The map of the Gradenbach catchment (32 km^2) illustrates five longitudinal subsystems (I-V) and four cirques (C1-C4) delivering sediments to the Gradenmoos basin (subsystem III). Ridges, crests, and escarpments are specified with linear symbols. The extent of the geomorphological map section shown in fig. 4 is specified additionally (rectangle). Major geologic units within the upper Möll catchment are indicated in map 2. Note the different topographic signatures of the Glockner, Goldberg, and Schober Range catchments apparent in the shaded relief.

with multiple cirques and hanging valleys framed by steep rockwalls and a stepped longitudinal valley profile characterised by knick points. In recent times, small glacier remnants but large areas potentially underlain by permafrost can be observed as a consequence of large but fragmented areas in high elevations, which are steeply inclined. According to modelling results using the empirical Permakart 3.0 model, 31% of the catchment is underlain by permafrost (Schrott & *alii*, 2012). The mean slope of these areas (41°) indicates that permafrost largely corresponds to rockwalls. Compared to neighbouring catchments (fig. 1, map 2) steepest average slope gradient (36.2°) and highest mean values of several morphometric parameters (*e.g.*, stream power index, terrain ruggedness index, relative relief) indicate enhanced rates of sediment production and transport within the catchment. Due to Pleistocene glacial erosion, pronounced over-steepening and over-deepening can be observed, whereas glacial scouring has been particularly effective within two confluence situations in the valley (Gradenalm, Gradenmoos basin; fig. 1, map 3). Major sediment sinks along the main channel prevent coarse-grained sediment throughput and account for the development of postglacial landscape archives showing different states of recent infilling. In the context of a cascading sedimentary system (Schrott & *alii*, 2003; Otto & *alii*, 2009), the catchment can be structured into five subsystems largely decoupled from each other (fig. 1, map 3).

As illustrated on the first historical map covering the study area (so-called «Kronlandskarte», 1834) the Gradensee marks the LIA extent of the main glacier in the valley (Gradenkees) and delimits the uppermost subsystem I (Valley Head; 4.3 km^2). The southern part of subsystem I encompasses two remnants of the heavily debris-covered Gradenkees, large frontal, basal and lateral moraines, and some talus sheets and cones underneath the rockwalls. Several post-LIA moraines and talus sheets are subject to periglacial creep leading to the development of active talus and debris rock glaciers. Fewer amounts of sediments are stored within a small cirque in the N of subsystem I, whereas the largest central part is dominated by bare rock and a patchy till cover. The undulated, glacially shaped subsystem II (Gradenseen; 1.8 km^2) is characterised by «*roches moutonnées*», a patchy till cover, and several small mires and lakes. Subsystem II covers the hydrological catchment area between the Gradensee and the Vordersee, a rockfall-dammed lake above the uppermost knick point in the longitudinal valley profile. With a small elevation range (2400-3100 m) subsystem II largely coincides with an amphibolite body incorporated in the mica-schist dominated lithology. Due to low topographic gradients

and a weathering resistant lithology, sediment storage is limited to smaller talus deposits underneath the rockwalls.

The major test site of this study – the Gradenmoos basin – corresponds to subsystem III. Located in the central catchment, it covers an area of 4.5 km^2 and ranges between 1920 m (basin floor) and 3283 m (Peak Petzeck) in elevation. The glacially over-deepened bedrock basin is the most pronounced sink in the catchment and is sharply delineated up- and downstream the Gradenbach creek. The bedrock steps bordering the basin might be caused by an increase in bedrock resistance (mica-schist *vs*. amphibolite), enhanced Pleistocene glacial erosion as a consequence of glacier confluence, and regional NW-SE oriented lineaments (Troll & *alii*, 1976) indicating a parallelism to these steps. As a consequence of longitudinal decoupling, sediment supply to the basin is largely restricted to four steep cirques (C1-C4, fig. 1, map 3). A variety of sediment storage landforms developed, including floodplain deposits and a peat bog covering the basin floor as well as hillslope deposits (debris cones, talus sheets) underneath the cirques and rockwalls surrounding the basin. In the context of a cascading sedimentary system, primary (*e.g.*, talus sheets; created by weathering and rockfall originating at the rockwall), secondary (*e.g.*, debris cones; created by the degradation of talus sheets located upstream through debris flows) and tertiary sediment storage landforms (*e.g.*, floodplain deposits; created by the fluvial reworking of secondary storages) can be differentiated. As will be shown, glacial and lacustrine processes also contributed to basin sedimentation in former times. The almost flat basin floor extends approx. 1 km in length (NE-SW) and 100-250 m in width (SE-NW) and can be structured in a proximal, central, and distal part. Low channel gradients and discharge velocities led to an anastomosing river pattern in the fully vegetated distal basin. Towards the central and proximal part, carrying capacity, frequency of channel migration, and surface grain sizes increase. This goes along with an increase in recent sediment transfer as indicated by fresh debris flow deposits delivered onto the floodplain during high runoff events. Based on a reconstructed ELA-depression of 180 m typical for climatically shielded, inner-Alpine regions (Kerschner, 2009), Lieb (1987) inferred that the Gradenmoos basin was ultimately ice-covered during the Younger Dryas (probably late-Egesen). The panoramic photo (fig. 2) illustrates the basin and major surrounding landforms, fig. 3 shows a TLS-based shaded relief image of the basin, and the geomorphological map of the area is presented in fig. 4.

Closeness of subsystem IV (Gradenalm; 6.5 km^2) is due to the damming effect of a debris cone partly covered by rockfall deposits. In contrast to subsystems I-IV, sediment transfer across subsystems IV and V might be less restricted during the Holocene due to unknown age of the valley-damming deposits and indefinite trap efficiency. Above the northern slope, subsystem IV encompasses two hanging valleys characterised by rockfall and rock glacier activity, huge amounts of sediment storage, and a low degree of sediment export. The southern valley flank in contrast shows steep rockwalls, low amounts of intermediate sediment storage, and mainly direct sediment supply to the hillslopes. The largest subsystem V (Valley Outlet; 14.6 km^2) drains the remaining eastern part of the catchment and includes two hanging valleys in the North, steep rockwalls and a smaller cirque in the South, and a deep-seated mass movement at the south-exposed outlet slope of the catchment. The latter mass movement was investigated in detail by several authors (*e.g.*, Brückl & Brückl, 2006; Brückl & *alii*, 2006; Weidner & *alii*, 2011). Within this easternmost subsystem V, the Gradenbach has to pass several control structures before draining in the river Möll.

METHODS

Within and surrounding the Gradenmoos basin (subsystem III), high-resolution surface (terrestrial laser-scanning, geomorphological mapping) and subsurface data (geophysical prospection, core drilling) has been acquired and used for subsequent GIS-based bedrock interpolation and 3-D modelling of sediment storage volumes. The timing of sedimentation and rockwall retreat after deglaciation and the differentiation of pre-Holocene basal till underneath present-day landforms are based on stratigraphic and palynological analyses of several sediment cores and AMS ^{14}C dating of organic core samples. Relevant issues for all methods applied will be described in the following, a detailed description can be found in Götz (2012).

FIG. 2 - Panoramic view into the Gradenmoos basin (view to SW, August 2009). Major landforms are indicated.

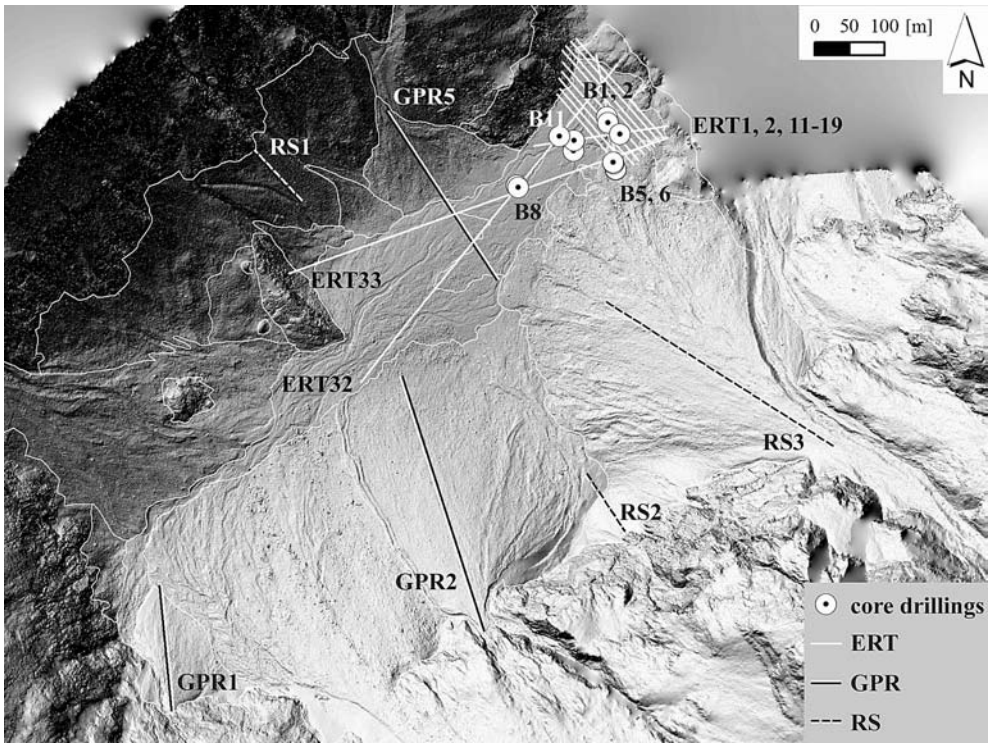

FIG. 3 - Locations of core drillings, 2-D resistivity (ERT), ground-penetrating radar (GPR), and refraction seismic (RS) survey lines in the Gradenmoos basin based on hillshaded TLS data (spatial resolution: 50 cm).

Geomorphological mapping

Geomorphological mapping serves as a key tool for an initial geomorphological system analysis and as an important basis to understand catchment configurations (Otto & Dikau, 2004; Smith & *alii*, 2011). A combined mapping approach covering the Gradenbach catchment was elaborated comprising a field and a GIS component. After a first site inspection in summer 2009, major landforms were digitised on orthophotos (1:5,000). During several subsequent field campaigns, sediment storage distribution was assessed manually with a minimum considered landform size of 100 m^2. Inaccessible areas (*e.g.*, steep cirques, some hanging valleys) were processed remotely using orthophotos. Field data was transferred into a GIS database and visualised as a first geomorphological map (1:10,000) covering subsystems I-III (17.4 km^2). This landform inventory created by Bellinger (2010) was extended to the entire catchment (32 km^2) and improved through further mapping campaigns in 2010 and 2011, multi-temporal orthophoto interpretation, and the analysis of airborne laser-scanning (ALS) data and derivatives (spatial resolution: 1 m), such as multidirectional shaded relief (Mark, 1992) or slope- and curvature grids. Particularly within the densely vegetated valley bottom, the adjacent through slopes, and within the North-exposed shadowy orthophoto areas, ALS data provided valuable additional information. The final inventory includes qualitative (*e.g.*, landform type, predominant processes of accumulation, vegetation cover, present-day sediment input, -output, and -throughput conditions) and quantitative data (*e.g.*, morphometric measures of slope gradient and elevation, planimetric (2-D) area, true (3-D) surface area) for each sediment storage landform, which are classified into rock glaciers, moraines, rock fall deposits, talus sheets and cones, debris cones, mass movements, alluvial fans and plains, mires, complex valley fill deposits within the hanging valleys, and *in-situ* weathered regolith. Remaining areas not covered by these landforms correspond to (heavily debris-covered) glaciers, lakes or bedrock. The area-wide polygonal data set covers the entire catchment and allows for a quick visualisation of multiple geomorphological data. Linear topographic features (crests, ridges, gorges, escarpments, moraine ridges) and point-based process information (mass movement, debris flow, rill erosion, rockfall and avalanches) were assessed additionally. A map section covering the Gradenmoos basin (subsystem III) is shown in fig. 4.

Terrestrial laser scanning (TLS)

A TLS survey was carried out in the Gradenmoos basin using a *Riegl LMS Z620i* instrument. Six scan positions were chosen in order to maximise point density, to balance point cloud homogeneity, and to minimise shadowing effects. The survey was based on 11 reflector cylinders (diameter: 11 cm; height: 10 cm) permanently installed in the field with positions widely distributed and visible from at least three scan positions. The procedure at each scan position comprises the acquisition of a sector scan (8-13x10^6 points, angular resolution: 0.039-0.041 deg), individual reflector scans with highest possible resolution, and the acquisition of photos covering the sector using a calibrated camera. In total, *ca.* 60.5x10^6 points were acquired. After data acquisition, the point clouds were spa-

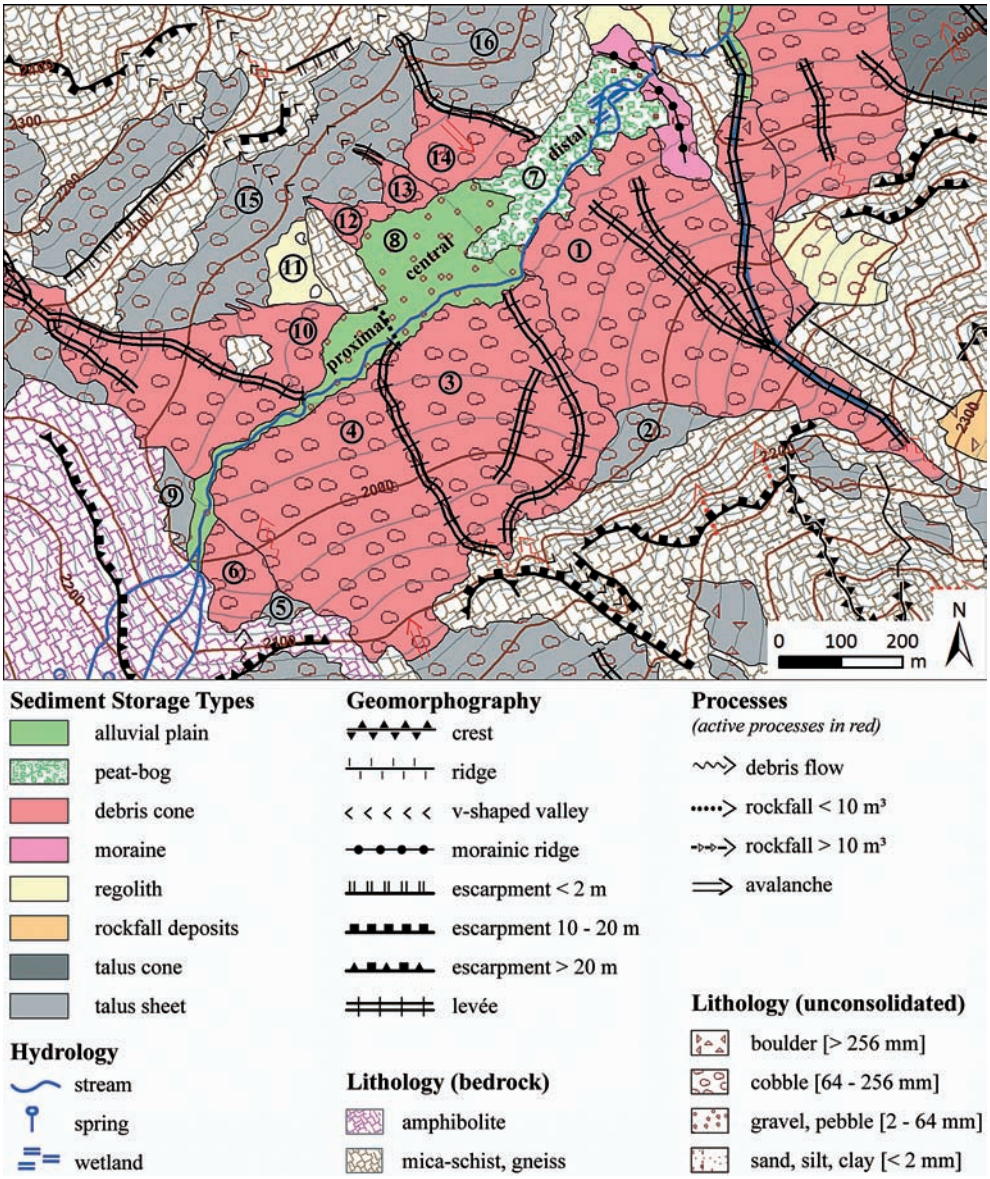

FIG. 4 - Geomorphological map of the Gradenmoos basin (subsystem III) providing information on form, process and material. Landform numbers as described in the text. Legend symbols refer to Kneisel & *alii* (1998) and Otto & Dikau (2004).

tially adjusted (registered) to each other by rotating and translating them. Registration accuracy is provided through standard deviations of reflector positions acquired from several scan positions. After registration the points refer to a common project coordinate system, which was converted into a global coordinate system (MGI Austria GK_M31) using DGPS-based reflector positions. Whereas data registration was achieved with a high level of accuracy (SD of residues: 1.9-3.6 cm), the conversion into the global coordinates yielded a higher standard deviation (40.1 cm) due to inaccuracies of DGPS positions. Despite of differential correction during post-processing, DGPS positions show a relatively large error (horizontal/vertical precision: 0.1-1.5 m/0.1-1.2 m), which is attributed to shadowing effects of the steep rockwalls, particularly nearby the reflector cylinders and to multipath effects. These raw LiDAR data were further processed in order to obtain triangulated meshes and gridded elevation data. First, the point cloud was cut to the area of interest before so-called 2.5-D filtering was applied, which decimates the point cloud and generates homogeneously resolved data set using a 'virtual grid' with an arbitrarily scalable cell size. According to view direction (in this case parallel to the Z-axis), the procedure maintains the position of the lowest point projected onto each grid cell. A small cell size of 10 x 10 cm was chosen, since 2.5-D filtering strongly impacts on steeply inclined surfaces. The filter is particularly effective nearby the scan positions with highest initial point densities and also eliminates vegetation to a certain extent. However, vegetation was finally eliminated manually by processing multiple cross slices of 10 m width. The resulting point cloud comprises *ca*. 14.5×10^6 points. With respect to the calculation of sediment storage volume, a first point cloud representing the current surface was decimat-

ed to 50x50 cm, triangulated, and true coloured with RGB information obtained by the camera. The resolution of a second point cloud, which is restricted to bedrock outcrops within the basin and the steep surrounding rockwalls, was further reduced to 5x5 m. GIS-based bedrock surface interpolation and quantification of sediment storage is based on this «bedrock point cloud» as well as geophysical and drilling information.

Core drilling, sampling, and AMS ^{14}C dating

Core drilling was applied to detect sediment thickness at single point locations in the basin, for validation of geophysical surveys, and – even if it is not the focus of this study – for a detailed analysis of the sedimentary evolution of the basin. Core drillings were performed using a gasoline powered percussion hammer (MK1, Atlas Copco) with an impact-energy of 60 joules and a frequency of 24 blows per second. A self-made, transportable drilling derrick facilitated drilling progress. Subject to variable subsurface conditions, open percussion gouges and core samplers with synthetic sampling tubes were used (length of each section: 1 m; diameter: 6 cm). A hydraulic puller was used to extract the sediment cores. Six successful drillings (B1, B2, B5, B6, B8, B11) could be carried down whereas remaining drilling attempts had to be aborted due to high resistances (fig. 3). To reconstruct postglacial basin evolution, the stratigraphy of the sediment cores was analysed (*e.g.*, grain size, colour, organics, lamination) and 21 organic samples (wood, branches) were dated (AMS ^{14}C, CEDAD laboratories, University of Salento, Italy). Calibration of conventional radiocarbon ages was performed using OxCal 3.10 based on the atmospheric dataset of (Reimer & *alii*, 2009). Presented ^{14}C ages correspond to the mean values within the 2σ probability range. Palynological analysis (cooperation with R. Krisai, University of Salzburg) was additionally performed throughout the sediment core B2 using a sample interval of 20 cm.

Geophysical prospection

To determine sediment thickness within and surrounding the basin, electrical resistivity tomography (ERT), ground-penetrating radar (GPR), and refraction seismic (RS) were applied. Since each technique makes use of a specific physical property of subsurface materials (*e.g.*, density, elastic moduli, permittivity, electrical conductivity), the suitability of a particular geophysical method is largely determined by the subsurface variability of the physical property to which the method responds (Schrott & Sass, 2008). To adjust survey design, geomorphological context and prior knowledge about site-specific subsurface conditions is crucial. In this context, the inverse relationship of data extent (penetration depth) and resolution – which is mainly controlled by survey length and electrode spacing in case of ERT, impact energy, survey length and geophone spacing in case of RS, or antenna frequency, survey length and the trigger interval in case of GPR – was carefully balanced for all methods applied. Geophysical prospection was adjusted to variable subsurface conditions as follows.

Within the water-saturated and fine-grained central and distal part of the basin, ERT yielded most meaningful raw data and realistic modelling results with just low residual errors. Since the quantification and postglacial evolution of the central part of the basin have been of particular interest (validated by core drilling), ERT was carried out most extensively. A multi-electrode device (Geotom MK1E100, Geolog2000) was used for data acquisition providing four channels with up to 25 electrodes each. The surveys were carried out with an electrode spacing of 4 m and total survey lengths from 140-596 m. Nine parallel lines (ERT11-19) and two intersecting ones (ERT1 and 2) were acquired in the distal part of the basin. ERT32 and 33 were carried out as roll-along surveys of 596 m length (3x396 m, 2x296 m overlap; fig. 3). Electrode positions were acquired using DGPS. The Wenner array was applied since it well resolves horizontally layered subsurface structures assumed beneath the basin floor. In order to enhance comparability, a uniform set of parameters was used for data inversion (Res2DInv, Geotomo).

Three refraction seismic (RS) surveys were acquired to detect thickness of hillslope deposits surrounding the basin using a 24-channel seismograph (Geode, Geometrics). RS profiles were positioned close to the rockwalls in order to improve modelling and data interpretation focusing on bedrock edge detection. Using 24 geophones and a spacing of 5 m, RS1 and RS2 resulted in total survey lengths of 115 m. The roll-along survey RS3 is based on 2x24 geophones, a spacing of 10 m, and a survey length of 430 m (overlap: 30 m; fig. 3). The signal was triggered using a 5 kg sledgehammer at each geophone position with a lateral offset of 50 cm. To improve signal-to-noise-ratio, the shots were stacked five times. Several long-range shots were acquired additionally beyond the survey limits at distances of 5-50 m to the start and endpoints of the profiles. Geophone positions were acquired using DGPS. Data processing (ReflexW; Sandmeier software) comprise picking of first arrivals for each shot and geophone position, the assignment of similarly inclined travel time segments to several layers, topographic correction, and the iterative process of refractor modelling. According to Hoffmann & Schrott (2003) a combined approach using wave-front inversion (WFI) and subsequent network ray tracing delivered most promising results.

Three ground-penetrating radar (GPR) surveys (length: 100-418.5 m, spacing: 0.5 m) were additionally acquired to derive thickness of hillslope storage landforms surrounding the basin using a MALA device (RAMAC/GPR Control Unit II) with an unshielded antenna system and a centre frequency of 50 MHz. GPR surveys started likewise at the apexes of the debris cones close to the rockwalls (fig. 3). ReflexW (Sandmeier software) was used for data processing. Applied processing steps comprise 1-D filters acting on single traces (subtract mean/dewow; bandpass frequency), 2-D filters acting on a range of traces or the entire survey line (background removal, AGC Gain), time-depths conversion (FK migration/Stolt), and topographic correction.

Modelling of sediment storage volumes

A point feature dataset was compiled from different sources as input for bedrock surface interpolation. Based on the most general assumption that the shape of bedrock at the surface is indicative for subsurface bedrock continuation, TLS-based bedrock coordinates (outcrops and steep rockwalls surrounding the basin) were integrated first. In a second step, geophysically determined bedrock positions were incorporated. In case of ERT, models with true XYZ coordinates were visualised as 2-D Delaunay surfaces within Paraview (Kitware) in order to extract bedrock coordinates using a resistivity threshold of 2 kΩm as discussed later. Bedrock edge from GPR and RS data was manually determined, positioned along the survey lines within a GIS, and incorporated in the data set used for interpolation. Three single bedrock coordinates derived from the core drillings B1, B2, and B11 were integrated last.

Interpolation of the bedrock interface is based on radial basis functions within ArcGIS 10 (ESRI) comprising several spline interpolation techniques. Splines were chosen as they fulfil two important preconditions in the context of the study. They are exact interpolators implying that positions of input points are preserved in the interpolated surface and they allow for the prediction of points located below the lowest sample and above the highest one, and thus allow for over-deepening and vertical exaggeration between the sample data. As a measure of how well the model predicts an interpolated surface, cross validation was carried out. For all input sample points the procedure successively omits a point, predicts its value, and compares it to the measured one. Errors between measured and predicted values (mean and RMS errors) served as basis to decide which model reproduced measured values with highest accuracy. Cross validation is further used by the software to optimise a so-called kernel parameter, which controls the degree of smoothness of the interpolated surface. Multiple models are evaluated and the kernel parameter, which yields the model with the lowest RMS error is chosen. Bedrock surfaces were interpolated using three kernel functions comprising thin plate spline (TPS), completely regularised spline (CRS) and multi-quadric functions (MQ), optimised kernel parameters and a multi-sectoral, circular search neighbourhood. In order to only evaluate prediction accuracies for bedrock coordinates derived from geophysical prospection and core drilling, cross validation was restricted to those. Bedrock surfaces were interpolated to grids (5x5 m) and converted to XYZ point data for subsequent volume calculations.

To maximise visual control, 3D landform volumes were calculated mesh-based within Riscan Pro (Riegl). A first volume is calculated between the upper (surface) mesh and a horizontal plane underneath. A second one corresponds to the volume between a lower (bedrock) mesh and the plane. The difference between both volumes within a specified landform extent conforms to the cut volume between both meshes, or to the landform volume, respectively. If the lower and upper surfaces intersect each other, also fill volumes are provided. Lower bedrock meshes were further decimated to 10x10 m using 2.5-D filtering in order to smooth artefacts produced by GIS-based interpolation. The upper surface in contrast is based on TLS-derived, triangulated meshes with a higher resolution of 50x50 cm. The horizontal plane below both meshes was located at an arbitrary elevation of 1800 m. The width and length of the «volumetric columns» between the meshes, which are summed up to calculate cut and fill volumes, were defined to 50 cm in order to balance accuracy and processing time. Landform cut volumes were finally reduced by volumes of pre-Holocene basal till, which are based on the landform extents and mean thicknesses of basal till (1.85 m) as observed by core drilling.

RESULTS

Sediment storage distribution

The geomorphological map section in fig. 4 indicates 16 sediment storage landforms within and surrounding the Gradenmoos basin. Debris cones (1, 3, 4, 6, 10, 12-14) and, to a minor extent, talus sheets (2, 5, 9, 15, 16) are predominant landform types surrounding floodplain deposits (8) and an Alpine lake mire (7) in the basin centre. Process-related point features (*e.g.*, rockfall, debris flow), linear topographic features (*e.g.*, escarpments, ridges, crests), as well as information on lithology (*e.g.*, bedrock type, grain sizes of unconsolidated deposits) and hydrology (*e.g.*, streams, springs, glaciers) are also provided.

Three smaller debris cones adjoin the basin to the N (12, 13, 14). Widely vegetated in present times, they show a minor degree of recent activity. With a larger extent and a higher recent activity, debris cone 10 developed underneath the cirques C1/2 (fig. 1). However, compared to the large debris cones 1, 3, and 4 underneath the steep cirques C3 and C4 in the S of the basin, cone 10 is supposed to store a relatively small amount of sediments. Debris cone 1 refers to the cirque C4 and shows distinct evidence to be created by multiple generations of debris flows. Typical patterns of debris flow tracks and '*levées*' can be observed at the recent surface showing different states of activity and vegetation coverage (fig. 3). In contrast, more homogeneous surface characteristics of the coalescing debris cones 3 and 4 indicate a greater influence of rockfall and avalanche activity responsible for sediment storage aggradation. Even though both cones imply a multi-process genesis, debris flow activity seems to have been the dominant process of accumulation. Presence of talus sheets in the steep cirque above and their dissection by gullies further indicate that large amounts of material stored in the cones must be attributed to remobilised sediment out of these sources delivered mainly by debris flows. Remaining landforms (2, 5, 9, 15, 16) refer to largely vegetated talus sheets, widely decoupled from the present-day sedimentary system. Due to size (2, 5, 9) and relatively shallow thickness (15, 16), they might store small amounts of sediments.

Stratigraphic, palynological and temporal information

Only selected results of the core drillings are described in the following with a focus on stratigraphic composition, depths and age of the basin fill. In total, six successful core drillings were carried down (B1, B2, B5, B6, B8, B11; fig. 1). Three of them reached bedrock in depths of 12.3 m (B1), 12.6 m (B2), and 23 m (B11) and cover the entire Holocene. Observed sediment thickness agrees with a sharp increase in subsurface resistivity and enabled to validate bedrock resistivity to 2 kΩm (fig. 5). Above bedrock edge, a shallow layer of basal till with an average thickness of 1.85 m was observed. This rather heterometric material is characterised by brownish colour, isolated pebbles in a fine matrix, and the absence of organic matter and pollen. As already proposed by Lieb (1987), the basin was probably glaciated for the last time during the Younger Dryas (Egesen oscillation) and postglacial sedimentation started afterwards, which is supported by early Holocene ^{14}C-ages of the lowest samples above basal till (B2/9.89 m: 10,375 cal. BP; B11/21.05 m: 9,475 cal. BP). Large sections between basal till and the beginning of moor formation near the surface show mainly clayey-silty, partly laminated deposits fading upwards to slightly coarser grain sizes. Already pointing towards a long-lasting lake in the basin, lake existence over a period of 7,500 years could be proved by palynology, since *Pediastrum* (a green alga inhabiting freshwater environments) appears above basal till until a depth of 3.60 m within the core B2. In direct subsequence *Equisetum* (horsetail) comes up, an indicator that the lake disappeared. Numerous layers of peat in the uppermost sections of the sediment cores above 1.75 m (B1, B2), 3.21 m (B11), and 4.27 m (B8) indicate that moor formation started between 2,870 cal. BP (B1, B2) and 2,066

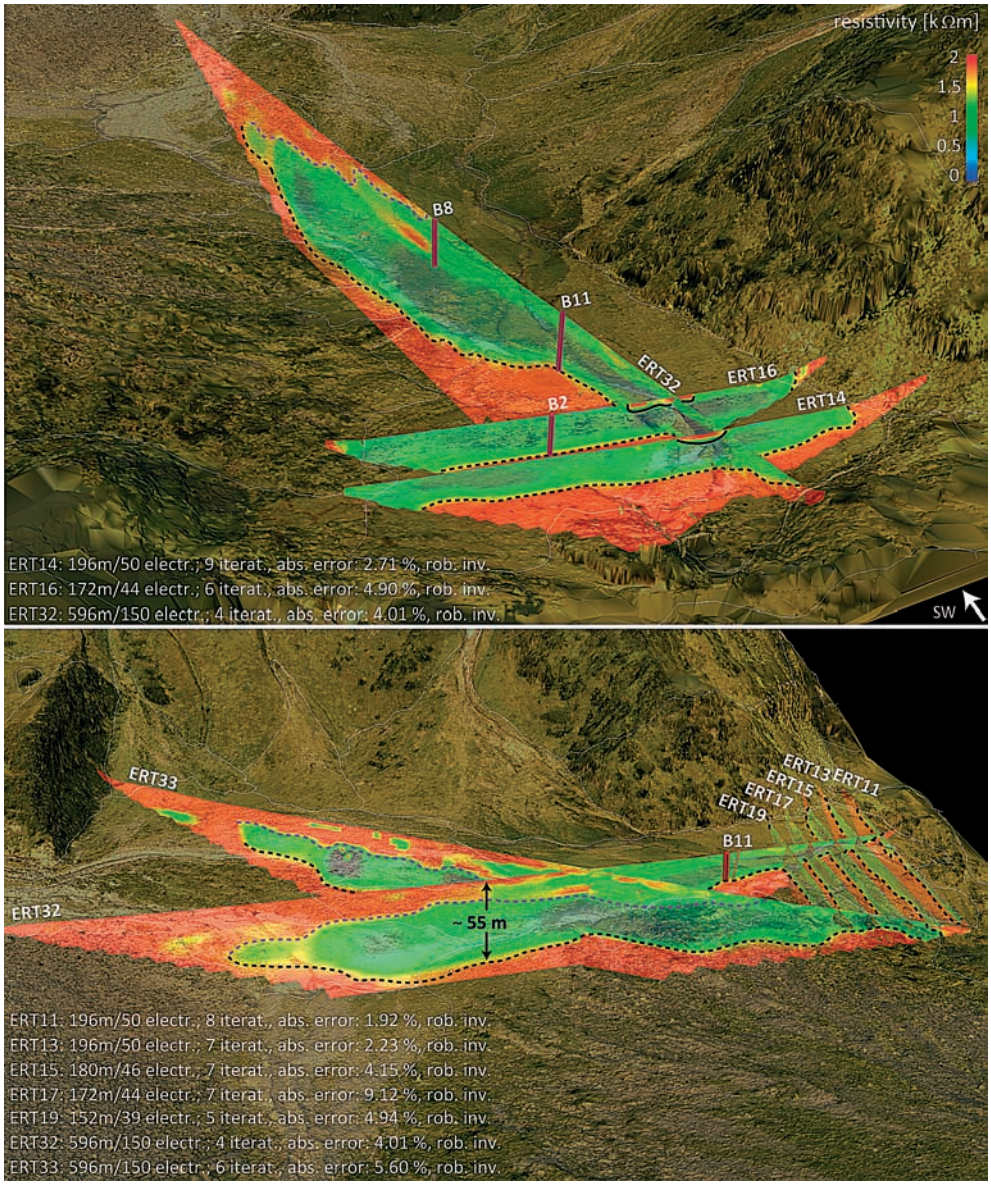

FIG. 5 - Selected resistivity tomographies and core drillings intersecting a semi-transparent, TLS-based surface mesh with true colour information. Dashed lines illustrate bedrock edge (black) and coarse-grained fluvial deposits overlying the fine-grained basin fill (purple) within the basin centre. Solid black lines (above) delimit coarser-grained channel deposits showing higher near-surface resistivities. Core drillings reaching bedrock are indicated red. Survey and inversion parameters and measures of model fit are given lower left (visualisation: Paraview).

cal. BP (B8). Well agreeing with these data, Krisai & *alii* (2006) dated this transition to 2,320 cal. BP (depth: 1.65 m) *ca*. 25 m apart from B1 and B2.

Geophysically derived subsurface information

As a consequence of water-saturated and fine-grained deposits overlaying bedrock, contrasts of subsurface resistivities are strong within the distal and central part of the basin. ERT accordingly delivered promising results and bedrock edge could be accurately detected. Conditions for successful ERT surveying decline towards the proximal part of the basin since depths to bedrock and near-surface resistivities increase, resistivity contrast decrease, and the injection of current gets hampered due to weak coupling conditions between the ground and the electrodes. Resulting tomographies show a sharp increase in resistivity with depth representing the bedrock interface. Bedrock depths derived from core drillings (B1, B2, B11) uniformly agree with the resistivity models and allow determining the local bedrock resistivity to 2 kΩm. ERT1, 2, and 11-19 indicate a successive increase of sediment thickness from 5-10 m (ERT11) to *ca*. 15 m towards the basin centre (ERT19). Bedrock edge within the deepest central part of the basin is provided by ERT32 and ERT33. Bedrock depth in ERT32 increases to 23 m at metre 130 (verified by B11) and finally drops to a maximum depth of around 55 m. The 3-D scene in fig. 5 illustrates selected tomographies and their agreement with bedrock depths derived from core drillings.

Resistivity models show low residual errors of 1.7-5.6% except for ERT17 (9.1%). Bedrock edge is continuously represented in the most distal tomographies (ERT11-14) but disappears at the northern and southern survey limits towards the basin centre (ERT15-19, see ERT16 in fig. 5). At the southern survey limits, this effect is explained by limited penetration depths and a well-continued bedrock surface underneath debris cone 1. Disappearance of bedrock edge at the northern survey limits is attributed to the steep dip of bedrock and to the weak resolution of vertical subsurface structures by the Wenner array. Central near-surface sections of ERT11-16 show isolated higher resistivities caused by coarser-grained channel deposits at the basin outlet. Towards the central basin, zones of increased near-surface resistivities widen and grow in thickness. This effect is attributed to enhanced channel dynamics and to a higher frequency of high magnitude flooding and debris flow events accumulating an uppermost less conductive layer characterised by fresh debris deposits and limited vegetation at the present surface.

Three RS surveys were carried out to detect thickness of hillslope deposits framing the basin to the N and S (RS1-3, fig. 3). After a steep drop of the bedrock interface close to the rockwalls, RS1 and RS2 yielded almost surface-parallel bedrock refractors in a depth of *ca*. 10 m indicating homogeneous sediment thicknesses for the investigated talus sheets (landforms 2, 15). The upper layers of both model sections show similar P-wave velocities of 0.3-0.45 km/s typical for Alpine talus deposits, whereas bedrock velocities range from 3.5 (RS1) to 5 km/s (RS2), likewise in the range of published data (*e.g.*, Brückl & *alii*, 2005). Bedrock edge underneath debris cone 1 (RS3; fig. 6) is detected at a maximum depth of 65 m. RS3 is best represented by a three-layer model with an intermediate layer of compacted debris and talus (1.1 km/s) and top and bottom layers similar to RS1 and RS2. As an estimate about the quality of the refractor models, RMS deviations between measured and calculated travel times are provided. Corresponding errors amount to 4.1% (RS1), 3.4% (RS2), and 6.4% (RS3).

Bedrock depths underneath debris cones 3, 6, and 14 were deduced from three GPR surveys starting at the apexes of the investigated cones (GPR1, GPR2, GPR5). Caused by low contrasts in permittivity between talus deposits and underlying bedrock, bedrock edge is not represented as a sharp reflector. Within comparable environments, Sass (2007) also reported weak and frequently absent reflectors at the talus-bedrock interface as a consequence of similar subsurface velocities in comparable subsurface units. However, despite of low dielectric contrasts and a lack of clear reflectors, the talus-bedrock interface frequently shows a characteristic fading of reflections (Sass, 2007) also observed within GPR1, GPR2 and GPR5. The interpreted bedrock edge drops nearby the rockwalls to reach sediment thicknesses of up to 35 m underneath debris cones 3 (GPR2; fig. 7), 6 (GPR1), and 14 (GPR5).

Sediment storage volumes

The surface structure of the bedrock interface generated, *i.e.* the degree of over-deepening and the surface roughness, is strongly affected by the interpolation technique applied. Whereas TPS interpolation delivers the visually most rugged surface, CRS provides the smoothest one. If total sediment volumes are compared, large differences in cut and fill volumes are observed. TPS delivers the largest cut (19.7×10^6 m^3) and the lowest fill volume (67×10^3 m^3) whereas CRS led to a smaller cut volume of 11.4×10^6 m^3 and a larger fill volume of 1.2×10^6 m^3. MQ derived volumes amount to intermediate values. If cut volumes are taken as 100%, the fractions of fill volumes amount to 0.3% (TPS), 2.3% (MQ), and 10.2% (CRS). Located along landform edges adjacent to bedrock outcrops and rockwalls, large parts of TPS-based fill volumes represent artefacts due to different spatial resolutions of the bedrock (10x10 m) and the landform surfaces (50x50 cm). In contrast to TPS interpolation, MQ, and particularly CRS produced unrealistic large fill volumes not only located along landform edges due to insufficient over-deepening between the sample data. Considering single sediment storage landforms, largest cut volumes (>10^6 m^3) refer to debris cones 1, 3, and 4 and to the fine-grained basin fill (landforms 7, 8). These landforms amount to 86% (TPS), 89% (MQ), and 92% (CRS) of total sediment storage within and surrounding the basin. Since geophysical data is limited to single landforms (1-3, 6-8, 14, 15) remaining landform volumes are strongly controlled by interpolation.

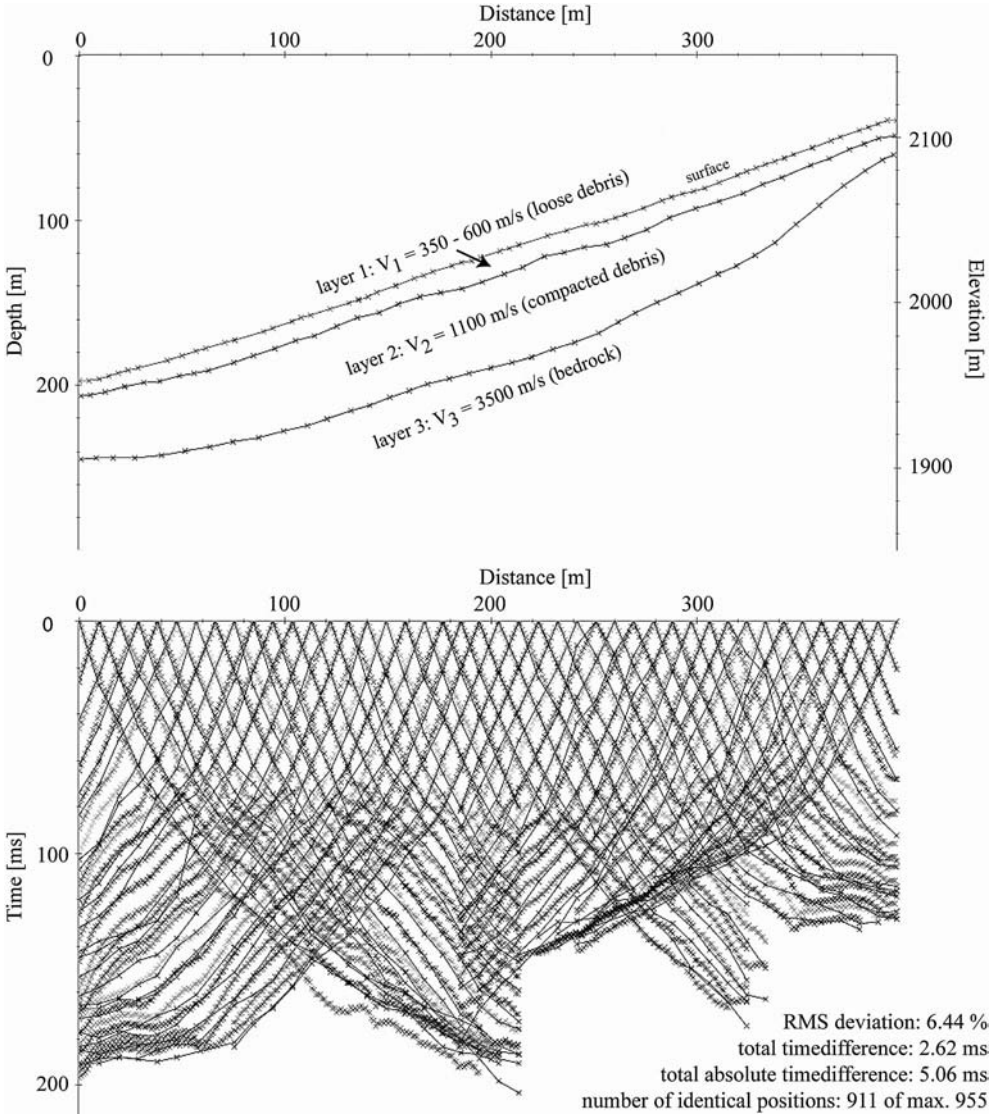

FIG. 6 - Above: Three-layer model derived from the refraction seismic survey RS3 underneath debris cone 1 (for location, see fig. 3). Modelling is based on wave-front inversion (WFI) and subsequent network ray tracing. Below: Measured (solid lines) *vs.* synthetic travel times (crosses) including the residual (RMS) error and numerical measures of model fit.

Fig. 8 illustrates the impact of geophysical data density on the scatter range of cut volumes. In case of landform 7, where highest data density is available (ERT and core drillings), similar cut volumes (1.13-1.21x10^6 m^3) and just small fill volumes (18-109 m^3) were obtained.

Several points indicate a most realistic bedrock surface produced by TPS interpolation:

(i) Mentioned ratios of cut and fill volumes provide evidence that MQ and CRS underestimate sediment storage since larger fill volumes are provided due to insufficient over-deepening.

(ii) Total cut volumes divided by the 2-D area of sediment storage delivers mean sediment thicknesses of 23.1 m (TPS), 14.8 m (MQ), and 9.7 m (CRS). Mean TPS-based landform thicknesses range from 3.5-40.3 m. In contrast, MQ and CRS provide mean thicknesses of 0.1-35.4 m and 0-30.7 m, respectively. Some landforms were used to qualitatively validate interpolation results, which is exemplified with landforms 11 and 15. Mapped as a shallow layer of regolith, landform 11 covers a relatively small and flat area adjacent to some bedrock outcrops. A mean thickness of 3.46 m derived from TPS interpolation well agrees with expected values, whereas MQ and CRS interpolation delivers obviously too small values of 0.1 and 0 m. The same applies for landform 15, a fully vegetated talus sheet, which is composed of shallow talus (max. 10 m) as specified by refraction seismic (RS1, fig. 3). In contrast to MQ (3 m) and CRS (1.6 m), TPS interpolation again delivered a realistic mean sediment thickness of 7.5 m.

(iii) As a numerical measure of how well the interpolation models predict the bedrock surface, cross validation was carried out. The procedure was limited to geophysically derived bedrock points since the entire data set would yield an apparent degree of accuracy. The procedure comprised 1527 points and delivered a smallest mean error (–0.014 m), a smallest standard deviation of errors (0.956 m), and lowest absolute errors in case of TPS interpolation. However, single large error values correspond to

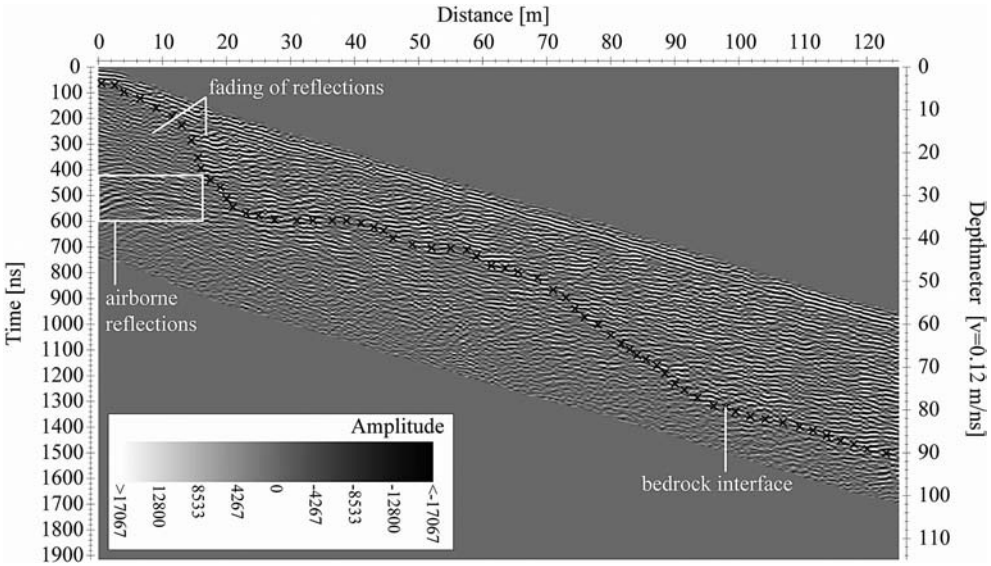

FIG. 7 - The uppermost 125 m of GPR2 illustrating the interpreted bedrock edge underneath debris cone 3 (for location, see fig. 3) as a consequence of fading patterns.

those bedrock points, where geophysical surveys intersect and bedrock depths not exactly match each other.

(iv) Postglacial sediment storage was derived from landform cut volumes corrected by a fraction of basal till. Even if field evidence is restricted to the sediment cores B1, B2, and B11, we assume that a layer of basal till which covers the entire basin with a mean thickness of 1.85 m. Till volumes (1.85 m x 2-D landform area) also point to an underestimation of sediment storage provided by MQ and CRS since the amount of basal till overbalances the cut volumes of landforms 2, 5, 9, 10, 11, 15 (in case of CRS) or 5 and 11 (in case of MQ). In contrast, all TPS-derived landforms provide «enough space» to capture partial volumes of basal till.

The total TPS-based sediment volume amounts to 19.7×10^6 m^3. Reduced by the share of pre-Holocene basal till (1.4×10^6 m^3 or 8% of total basin storage), postglacial sediment storage decreases to 18.3×10^6 m^3. TPS-based landform cut volumes are visualised as a 3-D scene in fig. 9.

Postglacial denudation and rockwall retreat

Rates of postglacial mechanical denudation ($DR_{mech.}$) and rockwall retreat were calculated on the basis of the equation:

$$DR_{mech} = SV\ \rho_s / (\rho_b \,.\, A \,.\, T) \qquad \text{(Eq. 1)}$$

using postglacial TPS-based landform cut volumes (SV), specific 2-D and 3-D source areas (A) as specified below, and a time increment (T) of 11 ka since a minimum age of *ca.* 10.4 ka cal. BP is provided by radiocarbon dating. According to literature values (*e.g.*, Brückl & *alii*, 2005; Sebastian, 2009), the rates are further based on a bedrock density (ρ_b) of 2.8 g/cm^3 and a porosity of sediment (ρ_s) of 2 g/cm^3.

Sediment supply to the basin is largely restricted to four steep cirques (C1-C4). In the context of a cascading sedimentary system, primary talus deposits developed within the cirques through weathering and rockfall processes. The degradation and redeposition of these deposits

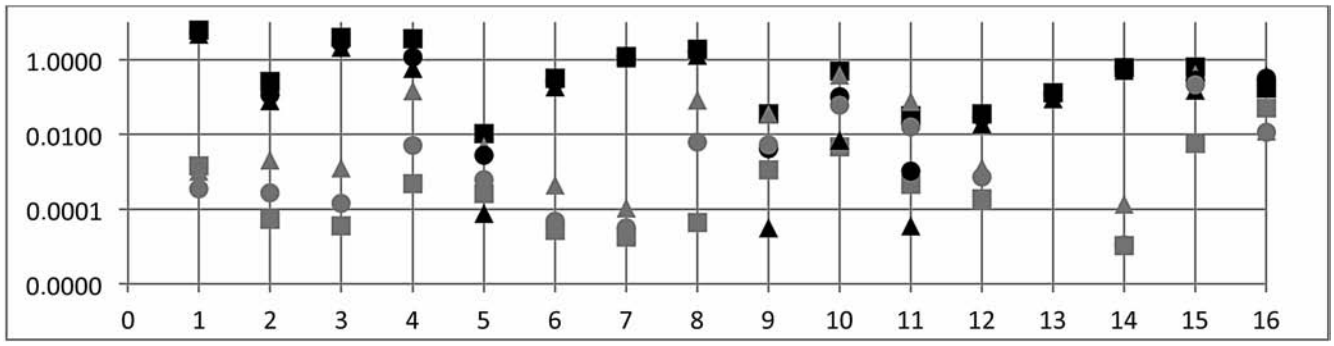

FIG. 8 - Cut (black) and fill (grey) volumes of the 16 investigated sediment storage landforms based on the three interpolation methods applied (TPS: squares; MQ: circles; CRS: triangles) plotted on a log scale. TPS interpolation delivered largest cut and lowest fill volumes. Largest landform volumes (>1 Mm^3) refer to debris cones 1, 3, 4 and the fine-grained basin fill (landforms 7, 8). Smallest scatter of cut volumes and smallest fill volumes are observed if geophysical data density is high (*e.g.*, landform 7).

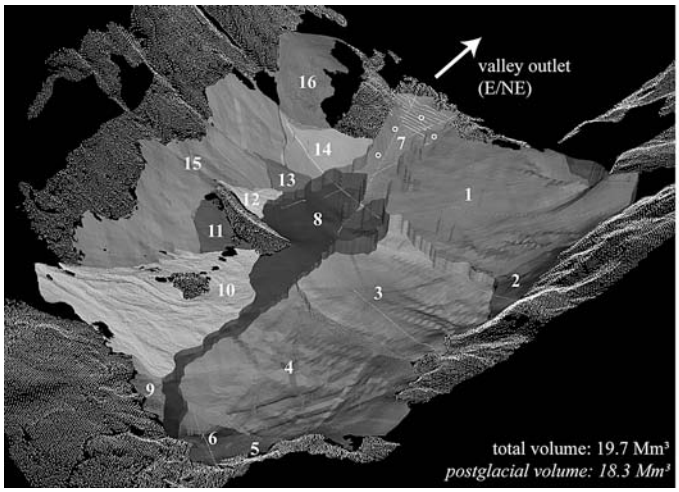

land-form [nr]	total volume [10^6 m³]	postgl. volume [10^6 m³]	mean thickness [m]
1	6.26	5.97	40.28
2	0.26	0.24	19.08
3	3.90	3.71	37.11
4	3.67	3.46	32.19
5	0.01	0.01	4.19
6	0.32	0.29	22.52
7	1.21	1.15	32.79
8	1.91	1.80	31.28
9	0.03	0.02	5.90
10	0.50	0.35	6.22
11	0.03	0.01	3.46
12	0.04	0.03	6.85
13	0.13	0.12	23.20
14	0.60	0.56	29.43
15	0.63	0.47	7.45
16	0.17	0.08	3.59

FIG. 9 - TPS-based cut volumes of the landforms 1-16 within and surrounding the Gradenmoos basin. Bedrock points used for interpolation (white) comprise TLS-derived bedrock outcrops and rockwalls as well as bedrock points derived from geophysical surveying and core drilling (circles). Geophysical data and drilling evidence are available for landforms 1, 2, 3, 6, 7, 8, 14 and 15. Total and postglacial landform volumes and mean thicknesses are provided. For scale see fig. 4 (visualisation: Paraview).

through mainly debris flows account for the accumulation of large secondary debris cones (landforms 1, 3, 4, 10) underneath the cirques. Tertiary basin fill deposits are finally caused by fluvial reworking of secondary debris cone deposits and by direct sediment supply to the fluvial system through single high-magnitude debris flow events. Debris cone 1 is supplied from cirque C4, cone 10 is concertedly supplied from C1 and C2, and the cones 3 and 4 are delivered from C3. Local source-sink relationships including the spatial pattern of primary, secondary and tertiary sediment storage landforms are illustrated in fig. 10.

Subject to specific source areas and associated sediment storage landforms, three scenarios of mechanical denudation and rockwall retreat are calculated. Since denudation rates are frequently based on planimetric (2-D) source areas whereas rates of rockwall retreat commonly refer to real DEM-derived (3-D) source areas, resulting rates are provided based on both measures.

In a minimum scenario A, sediment volumes are restricted to the large secondary debris cone deposits. Areas of primary talus storage within the cirques add to the source area. Both factors result in reduced rates of mechanical denudation. Scenario B delivers true rockwall retreat rates as primary cirque storage is taken into account and the source area is restricted to bare rock (walls). The quantification of talus in the cirques is based on the 3-D area and an approximated thickness of 3 m. In case of C3 and C4, this estimate is assumed to be realistic due to ground truth (heavily gullied talus sheets with intermediate bedrock outcrops) and is supported by steep average cirque slopes of 43-48° preventing the accumulation of

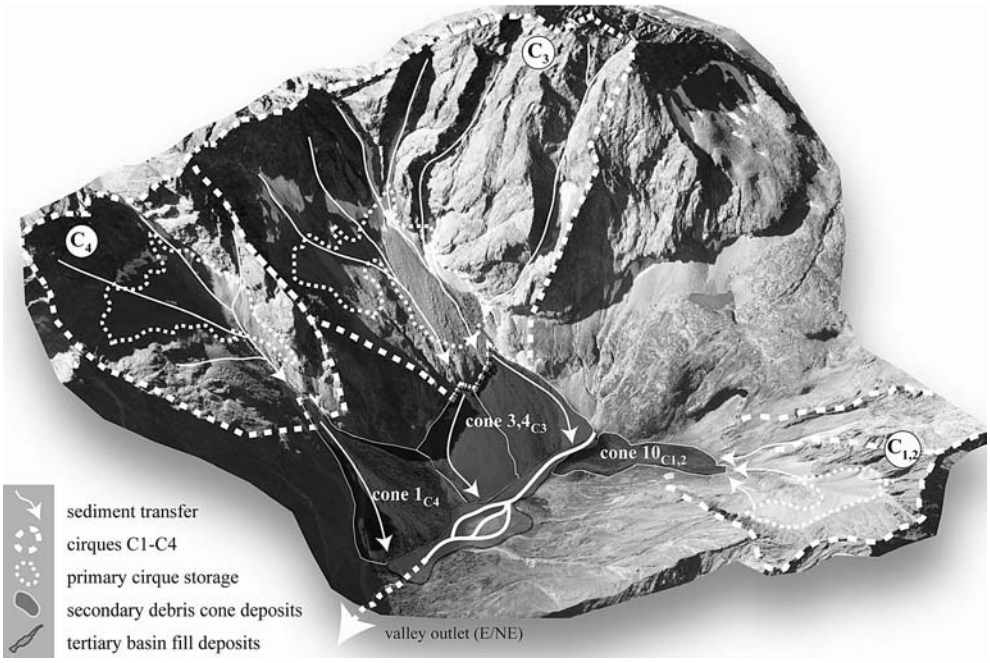

FIG. 10 - View into the Gradenmoos basin. The spatial arrangement of source areas (cirques C_1-C_4), areas of primary talus storage within the cirques, associated secondary debris cones (1, 3, 4, 10), and tertiary basin fill deposits are indicated. Sediment transfer paths are further illustrated. For scale, see fig. 4.

huge talus thickness. However, in case of C1/C2, the volume might be underestimated using a mean thickness of 3 m, since areas of primary talus storage within the cirques are larger and less steep. As sediment input from subsystem II further upstream has been effectively prevented during the Holocene, the majority of tertiary fine-grained basin fill deposits might have originated in the cirques as well. Even if it remains uncertain to which extent C1-C4 contributed to these tertiary deposits, a weighted approach was chosen and the basin fill was allocated to the cirques according to their size (3-D surface area; fig. 11). Scenario C takes this share additionally into account and consequently delivers highest rates of postglacial rockwall retreat. Scenario C might therefore reflect the investigated denudation-accumulation system most adequately and corresponding rates are considered to be most realistic.

Rates of mechanical denudation and rockwall retreat increase from scenario A to C (fig. 11) and range from 20-160 mm/ka (C1/2), 230-360 mm/ka (C3), and 320-520 mm/ka (C4). Steep cirque slopes account for significantly larger rates of 30-260 mm/ka (C1/2), 370-610 mm/ka (C3), and 520-930 mm/ka (C4) if 2-D source areas are considered. In contrast to similar rates observed for the cirques C3 and C4, C1/C2 yielded lower rates, which might be based on an underestimation of both, the volume of primary talus storage within the cirques and the volume of the associated debris cone 10, which is not validated by geophysical or drilling evidence.

DISCUSSION

Potential sources of errors

Results of this study are subject to potential errors from different sources, which can be roughly classified into environmentally and methodologically caused uncertainties. With respect to the former, the share of exported dissolved sediment load remains unknown but due to the low solubility of the mica-schist and amphibolite-dominated lithology, the amount is assumed to be of minor importance. Presented rates neglect this share and refer to mechanical denudation in the sense of Einsele (2000). In contrast, large parts of suspended river load and bedload have been trapped in the basin, since lake existence after deglaciation could be proved over a time period of 7500 years.

Difficult to separate from each other in a universal mathematical way, several methodological uncertainties need to be considered. Acquisition of surface data by means of geomorphological mapping, TLS, as well as DGPS-based survey localisations is supposed to involve errors of minor importance, since sediment storage landforms are clearly delineated and precisions of both the differential correction of GPS measurements and TLS-based point cloud matching provide error ranges of centimetres to decimetres. Acquisition and processing of subsurface data in contrast affect the results to a higher degree. Whereas the central basin fill is quantified most accurately, volumes of surrounding hillslope deposits are subject to larger inac-

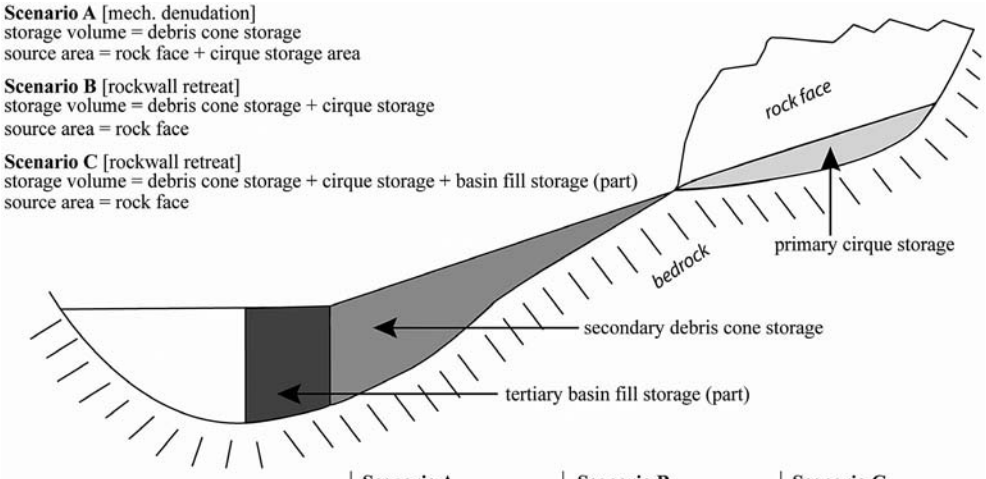

	Scenario A [mech. denudation]			Scenario B [rockwall retreat]			Scenario C [rockwall retreat]		
cirques	**C4**	**C3**	**C1/2**	**C4**	**C3**	**C1/2**	**C4**	**C3**	**C1/2**
source area 3-D - A [km²]	1.22	2.03	1.36	0.95	1.72	0.98	0.95	1.72	0.98
source area 2-D - A [km²]	0.75	1.26	0.9	0.53	1	0.6	0.53	1	0.6
storage volume - V [10^6 m³]	5.97	7.17	0.35	6.78	8.11	1.49	7.56	9.41	2.35
sediment yield - SY [m³/a]	543	652	32	617	737	135	687	855	214
bedrock density - ρ_b [g/cm³]	2.8	2.8	2.8	2.8	2.8	2.8	2.8	2.8	2.8
porosity of sediments - ρ_s [g/cm³]	2	2	2	2	2	2	2	2	2
time increment - T [ka]	11	11	11	11	11	11	11	11	11
rate 2-D [mm/ka]	520	370	30	830	530	160	930	610	260
rate 3-D [mm/ka]	320	230	20	460	310	100	520	360	160

FIG. 11 - Above: Schematic 2-D sketch of rockwall retreat scenarios. Below: Rates of mechanical denudation (scenario A) and rockwall retreat (scenarios B and C).

curacies. This can be attributed to the highest density, quality and reliability of geophysical data in the central and distal part of the basin and to the possibility of validating bedrock resistivity by core drillings. In contrast, a lower geophysical data density and a lack of complementary subsurface information cause larger uncertainties for volume estimations of hillslope deposits surrounding the basin. The comparison of single landform volumes derived from different interpolation techniques (fig. 8) reflects this effect and shows an increasing similarity of volumes with growing data density (*e.g.*, landform 7). The correction of total sediment storage by the share of pre-Holocene basal till underneath present-day landforms involves another simplification since an average till thickness of 1.85 m was derived from three core drillings (B1, B2, B11) and extrapolated to the entire basin. A final restriction appears for single landform volumes, which are based on the «vertical clipping» of mapped landform extents since various forms of subsurface landform interlocking are neglected.

A minimum temporal estimate of around 10.4 ka available for postglacial sedimentation and denudation is provided by radiocarbon dating. This time period was slightly prolonged to 11 ka, since the lowest sample taken for radiocarbon dating was located 40 cm above the transition from pre-Holocene basal till to lake deposits above. Furthermore, provided ^{14}C ages mark the death of these plants rather than the time of deposition. Even if not discussed in full detail here, the temporal evolution of the basin could be accurately reconstructed by means of 21 coherent radiocarbon ages as well as palynological and stratigraphic information making associated temporal uncertainties comparatively small.

Interpretation of denudation and rockwall retreat

The large range of published rates of Alpine denudation and rockwall retreat spans from 60-4000 mm/ka (various authors, tab. 1). Besides variable environmental char-

TABLE 1 - Above: Selected denudation rates for alpine catchments of different size and the entire Alps published by various authors. Underlying approaches (SB: sediment budget; CN: cosmogenic nuclides) and integration times are provided. Below: Selected rates of postglacial rockwall retreat derived from single talus landforms and associated source areas (various authors). Rates observed in gneiss and mica-schist lithologies are given bold type; rates from outside the Alps are given italic type (CH: Switzerland; A: Austria; I: Italy; F: France; G: Germany; PK: Pakistan)

Location	Denudation rate [DR; mm/a]	Integration time	Reference
This study	**30-930 (SB)**	**Postglacial**	
Turtmann Valley (CH)	**620-1870 (SB)**	**Postglacial**	**(Otto & *alii*, 2009)**
Hungerlitaelli (CH)	**1420-2640 (SB)**	**Postglacial**	"
Brändjitaelli (CH)	**1070-1840 (SB)**	**Postglacial**	**(Knopp, 2001)**
Walensee (CH)	>1500 (SB)	15 ka	(Müller, 1999)
Upper Rhône Valley (CH)	950 (SB)	Late and Postglacial	(Hinderer, 2001)
Inn (CH-A)	570 (SB)	Late and Postglacial	"
Alps	130 (SB)	Present	"
Alps	1760 (SB)	Lateglacial	"
Alps	620 (SB)	Late and postglacial	"
Alpenrhein (CH)	700-4000	Postglacial	(Korup & Schlunegger, 2009)
Bündner Rhine (CH)	580	Quaternary	(Jäckli, 1957)
Vallunga (I)	1100 (SB)	Postglacial	(Schrott & Adams, 2002)
Reintal (G)	300 (SB)	Postglacial	(Hufschmidt, 2002)
Crystalline Swiss Alps (CH)	900±300 (CN)	0.4-1.5 ka	(Wittmann & *alii*, 2007)
Rhone Tributaries (CH)	61±7.8-2120±940 (CN)	0.3-8.2 ka	(Norton & *alii*, 2010)
Holler (A)	**650±110 (CN)**	**1110±190**	**(Norton & *alii*, 2011)**
Holler 2 (A)	**1090±470 (CN)**	**660±280**	"
Krimmler (A)	**537±95 (CN)**	**1310±230**	"
Tauern (A)	**1240±240 (CN)**	**570±110**	"
Ecrins-Pelvoux massif	270-1070 (CN)	446-2573	(Delunel & *alii*, 2010)
Location	**Rockwall retreat rate [RRR; mm/a]**	**Integration time**	**Reference**
This study	**20-520 (SB)**	**Postglacial**	
Turtmann Valley (CH)	**120-3100 (SB)**	**Postglacial**	**(Otto & *alii*, 2009)**
Turtmann Valley (CH)	**1076 (SB)**	**Postglacial**	**(Otto & Sass, 2006)**
Reintal (G)	100-1000 (SB)	Postglacial	(Hoffmann & Schrott, 2002)
Reintal (G)	250-800 (SB)	Postglacial	(Sass, 2007)
Hoher Ifen (A)	350-1000 (SB)	Postglacial	"
Parzinn (A)	150-800 (SB)	Postglacial	"
Wolfeben (A)	200-500 (SB)	Postglacial	"
Kühtai (A)	**350-1000 (SB)**	**Postglacial**	"
Turtmann Valley (CH)	**600-1200 (SB)**	**Postglacial**	"
Bavarian Alps (G)	60-730 (SB)	Postglacial	(Sass & Wollny, 2001)
Eastern Pyrenees	*85-1580 (SB)*	*20-11.5 ka BP*	*(Delmas & alii, 2009)*
Sierra Nevada (USA)	*20-1220 (SB)*	*Postglacial*	*(Moore & alii, 2009)*
Nanga Parbat (PK)	*100-7000 (SB)*	*Postglacial*	*(Shroder & alii, 1999)*
Longyeardalen (Svalbard)	*330-1960 (SB)*	*Postglacial*	*(Siewert & alii, 2012)*

acteristics of the study sites, different methodological approaches covering various spatial and temporal scales with varying levels of detail need to be considered if the values are compared to each other. In case of cosmogenic nuclides (CN) based rates (*e.g.*, von Blanckenburg, 2006; Wittmann & *alii*, 2007; Delmas & *alii*, 2009; Delunel & *alii*, 2010; Norton & *alii*, 2010, 2011), the integration time is controlled by the rate itself and decreases with growing rates. High rates of 500-1500 mm/ka typically observed in the Alps account thus for relatively short integration times of 400-1200 years limiting the applicability of the method for the quantification of Holocene denudation. In a paraglacial context, CN-based rates should thus be lower as sediment budget (SB) based rates covering the entire postglacial period. On the other hand, CN-based rates include the chemical component often neglected in SB-based rates, raising the resulting values. Additionally, CN-based rates in small Alpine catchments might yield a large scatter and apparently too large values due to the lowering of ^{10}Be concentrations through disturbing effects, as for instance debris flow events, landsliding, or the incorporation of shielded or buried material (Niemi & *alii*, 2005; Kober & *alii*, 2012). If the rates are based on the sediment budget approach, (i) the time period available for postglacial sedimentation and denudation, (ii) the amount of exported sediment from a system, (iii) the storage quantification technique, (iv) the definition and delineation of the denudational area, and (v) the changing ratio of source and sediment storage areas through postglacial times strongly affect the results. The large scatter of Alpine denudation and rockwall retreat (tab. 1) might thus derive from both, variable environmental characteristics and changing predominance of different process domains within the investigated catchments (Caine, 2004), as well as from different methodological-technical approaches covering different spatial and temporal scales with varying levels of detail.

Lithological parameters strongly influence denudation and rockwall retreat (Moore & *alii*, 2009; Palumbo & *alii*, 2009; Norton & *alii*, 2011; Siewert & *alii*, 2012) assumed to cause a fragmented denudation pattern in the Alps. Since quantitative data on Holocene rockwall retreat in Alpine environments is limited and focusing on limestone and dolomite dominated catchments/rockwalls, the dataset needs to be enlarged and supplemented by further studies in different lithologies. Based on available data, slightly higher rates can be so far observed for gneiss and micaschist dominated catchments (tab. 1, bold).

Rates of rockwall retreat observed in this study (<520 mm/ka) rather agree with the lower range of published data even if they were expected to reach higher values due to lithologic, topographic, morphometric, and topo-climatic characteristics of the studied catchment (heavily fractured Palaeozoic lithology characterised by intensive weathering; distinct glacial signature with multiple cirques and hanging valleys; steep average slope gradient; small glacier remnants but large and steeply inclined areas potentially underlain by permafrost). Different explanations can be considered for the comparatively low rates observed. On the one hand, previous studies might have overestimated postglacial sediment storage and rockwall retreat as a consequence of the quantification technique used, ranging from simple visual estimation to geometrical models, drilling and coring, and detailed geophysical prospection (*e.g.*, André, 1997; Hinderer, 2001; Kuhlemann & *alii*, 2001; Hoffmann & Schrott, 2003; Curry & Morris, 2004; Delmas & *alii*, 2009; Moore & *alii*, 2009; Otto & *alii*, 2009; Tunnicliffe & Church, 2011). The neglect of pre-Holocene basal till underneath present-day landforms or the disregarding of the porosity of sediments might further account for enlarged volumes and thus to an overestimation of denudation and rockwall retreat. Increased rates of rockwall retreat could be also explained by simplified techniques to delineate and quantify 3-D rockwall source areas. In this context, underestimated 3-D rockwall source areas, as a consequence of lower DEM resolution or different calculation routines, cause larger rates and vice versa. An overestimation of published rates may also arise from the neglect of the shifting ratio between increasing sediment storage volumes and decreasing source areas through time. However, despite an assumed high level of accuracy, volumes of hillslope storage landforms and corresponding rates of rockwall retreat might be slightly underestimated in this study.

CONCLUSIONS

Total and postglacial sediment storage was quantified within and surrounding the glacially overdeepened Gradenmoos basin (4.5 km^2) in the central Gradenbach catchment (32 km^2, Schober Range, Austrian Alps) using high-resolution surface data (terrestrial laser scanning, geomorphological mapping), direct (core drilling) and indirect subsurface information (electrical resistivity tomography, ground-penetrating radar and refraction seismic), as well as GIS and 3-D modelling. Rates of rockwall retreat and mechanical denudation are based on these data and a time period of postglacial sedimentation and denudation derived from core drilling, stratigraphic and palynological analyses, and radiocarbon dating. Most important outcomes of this study are as follows:

– The onset of sediment storage aggradation after deglaciation was determined to approx. 11 ka BP by means of radiocarbon ages obtained from the drilling cores and complementary stratigraphic and palynological information.
– The latest lateglacial Egesen oscillation effectively scoured the basin leaving only a shallow layer of pre-Holocene basal till. Its volume was approximated to 1.4×10^6 m^3 (*ca.* 8% of total basin storage) and excluded from the quantification of postglacial sediment storage and rockwall retreat.
– The postglacial sedimentary record in the basin is almost completely preserved due to lake existence after deglaciation for around 7500 years. Hence, output might be restricted to small amounts of dissolved load and to probably negligible amounts of suspended load during the late Holocene.

– Total (postglacial) sediment storage amounts to *ca*. 19.7 (18.3)x10^6 m^3, whereas single landform volumes range from 0.03 (0.01)-6.26 (5.97)x10^6 m^3.
– Hillslope storage landform volumes overbalance basin fill deposits by a factor of five.
– Three scenarios of mechanical denudation and rockwall retreat provide rates of up to 520 mm/ka considering 3-D source areas.

The study copes with several uncertainties ignored in previous studies (*e.g*., Hoffmann & Schrott, 2002; Sass, 2007; Otto & *alii*, 2009) comprising the approximation of pre-Holocene basal till underneath present-day landforms, the incorporation of primary, secondary and tertiary sediment storages (fig. 10, 11), and the timing of the period available for postglacial sedimentation and rockwall retreat. Despite rockfall-prone topographic, lithologic, and topo-climatic conditions, observed rates of rockwall retreat are relatively low if compared to published values. However, since comparable data is limited and based on different approaches covering a range of spatial and temporal scales with different levels of detail, further research on the topic needs to be carried out. On the one hand, the dataset on Alpine rockwall retreat needs to be extended and knowledge about the factors governing the process (*e.g*., rockwall slope, elevation, and exposition, rock-mass strength, influence of freeze/thaw cycles, influence of permafrost) needs to be enlarged. This might be carried out through further small-scale studies in similar environments but different lithologies. A larger sampling size might help to assess the effective scatter of Alpine rockwall retreat rather than a spatially averaged signal of denudation and might provide a better basis for the interpretation of rates derived from different approaches. A combined application of different quantification techniques within the same study sites is finally suggested in order to estimate the accuracy and comparability of the approaches and to improve the interpretation of Alpine landscape evolution through rates of denudation and rockwall retreat averaging over different time periods.

REFERENCES

André M.F. (1997) - *Holocene rockwall retreat in Svalbard: A triple-rate evolution*. Earth Surface Processes and Landforms, 22(5), 423-440.

Ballantyne C.K. (2002) - *Paraglacial Geomorphology*. Quaternary Science Reviews, 21, 1935-2017.

Bellinger J. (2010) - *Die Sedimentkaskade des oberen Gradentals, Hohe Tauern, Österreich.* Unpublished Diploma Thesis, Goethe-Universität Frankfurt, 80 pp.

Brückl E. & Brückl J. (2006) - *Geophysical models of the Lesachriegel and Gradenbach deep-seated mass-movements (Schober Range, Austria).* Engineering Geology, 83(1-3), 254-272.

Brückl E., Dresen L., Edelmann H.A.K., Fertig J., Gaertner H., Gelbke C., Kirchheimer F., Krummel H., Liebhardt G., Orlowsky D., Reimers L., Sandmeier K.-J., Schneider C., Utecht T. & Witka T. (2005) - *Seimik*. In: K. Knödel, H. Krummel & G. Lange (Eds.), «Geophysik. Handbuch zur Erkundung des Untergrundes von Deponien und Altlasten». Springer, Berlin, 425-726.

Brückl E., Brunner F.K. & Kraus K. (2006) - *Kinematics of a deep-seated landslide derived from photogrammetric, GPS and geophysical data.* Engineering Geology, 88(3-4), 149-159.

Caine N. (2004) - *Mechanical and chemical denudation in mountain systems.* In: Owen L.A. & Slaymaker O. (Eds.), «Mountain Geomorphology». Arnold, London, pp. 132-152.

Champagnac J.D., Schlunegger F., Norton K., von Blanckenburg F., Abbuhl L.M. & Schwab M. (2009) - *Erosion-driven uplift of the modern Central Alps.* Tectonophysics, 474(1-2), 236-249.

Cossart E. & Fort M. (2008) - *Consequences of landslide dams on Alpine river valleys: Examples and typology from the French Southern Alps.* Norsk Geogr Tidsskr, 62(2), 75-88.

Curry A.M. & Morris C.J. (2004) - *Lateglacial and Holocene talus slope development and rockwall retreat on Mynydd Du, UK.* Geomorphology, 58(1-4), 85-106.

Delmas M., Calvet M. & Gunnell Y. (2009) - *Variability of Quaternary glacial erosion rates - A global perspective with special reference to the Eastern Pyrenees.* Quaternary Science Reviews, 28(5-6), 484-498.

Delunel R., van der Beek P.A., Carcaillet J., Bourles D.L. & Valla P.G. (2010) - *Frost-cracking control on catchment denudation rates: Insights from in situ produced Be-10 concentrations in stream sediments (Ecrins-Pelvoux massif, French Western Alps).* Earth and Planetary Science Letters, 293(1-2), 72-83.

Einsele G. (2000) - *Sedimentary basins: evolution, facies, and sediment budget*. Springer, Heidelberg, 792 pp.

Einsele G. & Hinderer M. (1998) - *Quantifying denudation and sediment-accumulation systems (open and closed lakes): basic concepts and first results*. Palaeogeography Palaeoclimatology Palaeoecology, 140(1-4), 7-21.

Götz J. (2012) - *Quantification and Postglacial evolution of an inner alpine sedimentary basin (Gradenmoos Basin, Hohe Tauern).* PhD thesis, University of Salzburg, 125 pp.

Hales T.C. & Roering J.J. (2005) - *Climate-controlled variations in scree production, Southern Alps, New Zealand*. Geology, 33(9), 701-704.

Hergarten S., Wagner T. & Stuwe K. (2010) - *Age and Prematurity of the Alps derived from Topography*. Earth and Planetary Science Letters, 297(3-4), 453-460.

Hinderer M. (2001) - Late *Quaternary denudation of the Alps, valley and lake fillings and Modern river loads.* Geodinamica Acta, 14(4), 231-263.

Hinderer M. (2012) - *From gullies to mountain belts: A review of sediment budgets at various scales*. Sedimentary Geology, 280, 21-59.

Hinderer M. & Einsele G. (2001) - *The world's large lake basins as denudation-accumulation systems and implications for their lifetimes.* Journal of Paleolimnology, 26(4), 355-372.

Hoffmann T. & Schrott L. (2002) - *Modelling sediment thickness and rockwall retreat in an Alpine valley using 2D-seismic refraction (Reintal, Bavarian Alps).* Zeitschrift für Geomorphologie, N. F., Suppl.-Bd., 127, 153-173.

Hoffmann T. & Schrott L. (2003) - *Determining sediment thickness of talus slopes and valley fill deposits using seismic refraction - a comparison of 2D interpretation tools.* Zeitschrift für Geomorphologie, N. F., Suppl.-Bd., 132, 71-87.

Hufschmidt G. (2002) - *GIS-gestützte Modellierung von Sedimentspeichern als Komponenten eines alpinen Geosystems (Reintal, Bayrische Alpen).* Unpublished Diploma Thesis, University of Bonn, 106 pp.

Jäckli H. (1957) - *Gegenwartsgeologie des bündnerischen Rheingebiets. Ein Beitrag zur exogenen Dynamik alpiner Gebirgslandschaften*. Geotechnische Serie, 36. Kümmerle & Frey, Bern.

Jordan P. & Slaymaker O. (1991) - *Holocene sediment production in Lillooet river basin, British Columbia: a sediment budget approach*. Géographie Physique et Quaternaire, 45(1), 45-57.

Kerschner H. (2009) - *Gletscher und Klima im Alpinen Spätglazial und frühen Holozän, alpine space*. Man & environment, vol. 6: Klimawandel in Österreich. Innsbruck University Press, Innsbruck, 5-26.

Kneisel C., Lehmkuhl F., Winkler S., Tressel E. & Schröder H. (1998) - *Legende für geomorphologische Kartierungen im Hochgebirge.* Trierer Geographische Arbeiten, 18. Geographische Gesellschaft Trier.

KNOPP F. (2001) - *Untersuchungen zum Sedimenthaushalt eines hochalpinen Hängetals im Turtmanntal, Wallis, Schweiz*. Unpublished Diploma Thesis, University of Bonn, 123 pp.

KOBER F., HIPPE K., SALCHER B., IVY-OCHS S., KUBIK P.W., WACKER L. & HÄHLEN N. (2012) - *Debris-flow-dependent variation of cosmogenically derived catchment-wide denudation rates.* Geology, 40(10), 935-938.

KORUP O. & SCHLUNEGGER F. (2009) - *Rock-type control on erosion-induced uplift, eastern Swiss Alps*. Earth and Planetary Science Letters, 278(3-4), 278-285.

KRISAI R., MAYER W., SCHRÖCK C. & TÜRK R. (2006) - *Das Gradenmoos in der Schobergruppe (NP Hohe Tauern, Kärnten) Vegetation und Entstehung*. Carinthia II, 196(116), 359-386.

KRONLANDSKARTE (1834) - Blatt/sheet Section No.2, Westliche Collone No.IX der Landesaufnahme des Konigreichs Illirien (aufgenommen 1834 durch Czykanek).

KUHLEMANN J., FRISCH W., DUNKL I. & SZÉKELY B. (2001) - *Quantifying tectonic versus erosive denudation by the sediment budget: the Miocene core complexes of the Alps.* Tectonophysics, 330(1-2), 1-23.

LANG E. & HAGEN K. (1999) - *Wildbacheinzugsgebiet Gradenbach. Analyse des Niederschlag- und Abflußgeschehens 1968-1996*. FBVA-Berichte 108, Wien, 109 pp.

LIEB G. (1987) - *Die Gletscher und Blockgletscher im Kärntner Teil der Schobergruppe und ihre Entwicklung seit dem Spätglazial.* Unpublished PhD thesis, University of Graz, 286 pp.

MARK R. (1992) - *Multidirectional, oblique-weighted, shaded-relief image of the Island of Hawaii*. U.S. Geological Survey Open-File Report 92-422 Online version 1.0, 1-5.

MOORE J.R., SANDERS J.W., DIETRICH W.E. & GLASER S.D. (2009) - *Influence of rock mass strength on the erosion rate of Alpine cliffs.* Earth Surface Processes and Landforms, 34(10), 1339-1352.

MÜLLER B.U. (1999) - *Paraglacial sedimentation and denudation processes in an Alpine valley of Switzerland. An approach to the quantification of sediment budgets.* Geodinamica Acta, 12(5), 291-301.

NIEMI N.A., OSKIN M., BURBANK D.W., HEIMSATH A.M. & GABET E.J. (2005) - *Effects of bedrock landslides on cosmogenically determined erosion rates.* Earth and Planetary Science Letters, 237(3-4), 480-498.

NORTON K.P., VON BLANCKENBURG F. & KUBIK P.W. (2010) - *Cosmogenic nuclide-derived rates of diffusive and episodic erosion in the glacially sculpted upper Rhone Valley, Swiss Alps.* Earth Surface Processes and Landforms, 35(6), 651-662.

NORTON K.P., VON BLANCKENBURG F., DIBIASE R., SCHLUNEGGER F. & KUBIK P.W. (2011) - *Cosmogenic (10)Be-derived denudation rates of the Eastern and Southern European Alps.* International Journal of Earth Sciences, 100(5), 1163-1179.

OTTO J.C. & DIKAU R. (2004) - *Geomorphologic system analysis of a high mountain valley in the Swiss Alps.* Zeitschrift für Geomorphologie, 48(3), 323-341.

OTTO J.C. & SASS O. (2006) - *Comparing geophysical methods for talus slope investigations in the Turtmann valley (Swiss Alps)*. Geomorphology, 76(3-4), 257-272.

OTTO J.C., SCHROTT L., JABOYEDOFF M. & DIKAU R. (2009) - *Quantifying sediment storage in a high Alpine valley (Turtmanntal, Switzerland).* Earth Surface Processes and Landforms, 34(13), 1726-1742.

PALUMBO L., HETZEL R., TAO M. & LI X. (2009) - *Topographic and lithologic control on catchment-wide denudation rates derived from cosmogenic Be-10 in two mountain ranges at the margin of NE Tibet.* Geomorphology, 117(1-2), 130-142.

REID L.M. & DUNNE T. (Eds.) (1996) - *Rapid evaluation of sediment budgets*. GeoEcology paperback. Catena Verlag, GeoScience Publisher, Reiskirchen, 164 pp.

REIMER P.J., BAILLIE M.G.L., BARD E., BAYLISS A., BECK J.W., BLACKWELL P.G., RAMSEY C.B., BUCK C.E., BURR G.S., EDWARDS R.L., FRIEDRICH M., GROOTES P.M., GUILDERSON T.P., HAJDAS I., HEATON T.J., HOGG A.G., HUGHEN K.A., KAISER K.F., KROMER B., MCCORMAC F.G., MANNING S.W., REIMER R.W., RICHARDS D.A., SOUTHON J.R., TALAMO S., TURNEY C.S.M., VAN DER PLICHT J. & WEYHENMEYE C.E. (2009) - *Intcal09 and Marine09 Radiocarbon Age Calibration Curves, 0-50,000 Years Cal BP*. Radiocarbon, 51(4), 1111-1150.

RYDER J.M. (1971a) - *Some Aspects of Morphometry of Paraglacial Alluvial Fans in South-Central British Columbia.* Canadian Journal of Earth Sciences, 8(10), 1252-1264.

RYDER J.M. (1971b) - *Stratigraphy and Morphology of Para-Glacial Alluvial Fans in South-Central British-Columbia*. Canadian Journal of Earth Sciences, 8(2), 279-298.

SASS O. (2007) - *Bedrock detection and talus thickness assessment in the European Alps using geophysical methods.* Journal of Applied Geophysics, 62(3), 254-269.

SASS O. & WOLLNY K. (2001) - *Investigations regarding Alpine talus slopes using ground-penetration radar (GPR) in the Bavarian Alps, Germany.* Earth Surface Processes and Landforms, 26, 1071-1086.

SCHLUNEGGER F. & HINDERER M. (2003) - *Pleistocene/Holocene climate change, re-establishment of fluvial drainage network and increase in relief in the Swiss Alps*. Terra Nova, 15(2), 88-95.

SCHROTT L. & ADAMS T. (2002) - *Quantifying sediment storage and Holocene denudation in an Alpine basin, Dolomites, Italy.* Zeitschrift für Geomorphologie N.F. Suppl.-Bd., 128, 129-145.

SCHROTT L. & SASS O. (2008) - *Application of field geophysics in geomorphology: Advances and limitations exemplified by case studies.* Geomorphology, 93(1-2), 55-73.

SCHROTT L., HUFSCHMIDT G., HANKAMMER M., HOFFMANN T. & DIKAU R. (2003) - *Spatial distribution of sediment storage types and quantification of valley fill deposits in an Alpine basin, Reintal, Bavarian Alps, Germany*. Geomorphology, 55, 45-63.

SCHROTT L., OTTO J.-C. & KELLER F. (2012) - *Modelling Alpine permafrost distribution in the Hohe Tauern region, Austria*. Austrian Journal of Earth Sciences, 105/2, 169-183.

SEBASTIAN U. (2009) - *Gesteinskunde: Ein Leitfaden für Einsteiger und Anwender*. Spektrum, Heidelberg, 166 pp.

SHRODER J.F., SCHEPPY R.A. & BISHOP M.P. (1999) - *Denudation of small Alpine basins, Nanga Parbat Himalaya, Pakistan.* Arctic, Antarctic, and Alpine Research, 31(2), 121-127.

SIEWERT M.B., KRAUTBLATTER M., CHRISTIANSEN H.H. & ECKERSTORFER M. (2012) - *Arctic rockwall retreat rates estimated using laboratory-calibrated ERT measurements of talus cones in Longyeardalen, Svalbard*. Earth Surface Processes and Landforms, 37(14), 1542-1555.

SLAYMAKER O. (2003) - *The sediment budget as conceptual framework and management tool.* Hydrobiologia, 494(1-3), 71-82.

SLAYMAKER O. (2009) - *Proglacial, periglacial or paraglacial?* In: Knight J. & Harrison S. (Eds.), «Periglacial and Paraglacial Processes and Environments». The Geological Society, Special Publication 320, London, 71-84.

SMITH M., PARON P. & GRIFFITHS J. (2011) - *Geomorphological Mapping: Methods and Applications.* Elsevier Science & Technology, 610 pp.

TROLL G., FORTS R., SÖLLNER F., BRACK W., KOHLER H. & MÜLLER-SOHNIUS D. (1976): *Über Bau, Alter und Metamorphose des Altkristallins der Schobergruppe, Osttirol.* Geologische Rundschau, 65, 483-511.

TUNNICLIFFE J.F. & CHURCH M. (2011) - *Scale variation of post-glacial sediment yield in Chilliwack Valley, British Columbia.* Earth Surface Processes and Landforms, 36(2), 229-243.

VON BLANCKENBURG F. (2006): *The control mechanisms of erosion and weathering at basin scale from cosmogenic nuclides in river sediment.* Earth and Planetary Science Letters 242(3-4), 224-239.

WEIDNER S., MOSER M. & LANG E. (2011) - *Geotechnische und kinematische Analyse des Talzuschubes Gradenbach.* Jahrbuch der Geologischen Bundesanstalt, 151, 17-60.

WITTMANN H., VON BLANCKENBURG F., KRUESMANN T., NORTON K.P. & KUBIK P.W. (2007) - *Relation between rock uplift and denudation from cosmogenic nuclides in river sediment in the Central Alps of Switzerland*. Journal of Geophysical Research-Earth Surface, 112 (F04010. doi:10.1029/2006JF000729).

(Ms. received 15 December 2012; accepted 1 March 2013)